Bioorganic Chemistry 108 (2021) 104648

Contents lists available at ScienceDirect

Bioorganic Chemistry

journal homepage: www.elsevier.com/locate/bioorg

Discovery of 5-(3-bromo-2-(2,3-dibromo-4,5-dimethoxybenzyl)-4,5-dimethoxybenzylidene)thiazolidine-2,4-dione as a novel potent protein tyrosine phosphatase 1B inhibitor with antidiabetic properties

Bo Jiang [a,b,1], Jiao Luo [a,1], Shuju Guo [a,b], Lijun Wang [a,b,*]

[a] Key Laboratory of Experimental Marine Biology, Institute of Oceanology, Chinese Academy of Sciences, Qingdao 266071, China
[b] Center for Ocean Mega-Science, Chinese Academy of Sciences, 7 Nanhai Road, Qingdao 266071, China

ARTICLE INFO

Keywords:
Type 2 diabetes mellitus
Protein tyrosine phosphatase 1B inhibitors
Thiazolidinedione
Insulin signaling
Anti-diabetic activities

ABSTRACT

Protein tyrosine phosphatase 1B (PTP1B) is a well-validated target in therapeutic interventions for type 2 diabetes mellitus (T2DM), however, PTP1B inhibitors containing negatively charged nonhydrolyzable pTyr mimetics are difficult to convert to the corresponding *in vivo* efficacy owing to poor cell permeability and oral bioavailability. In this work, molecules bearing less acidic heterocycle 2,4-thiazolidinedione and hydantoin were designed, synthesized and evaluated for PTP1B inhibitory potency, selectivity and *in vivo* antidiabetic efficacy. Among them, compound **5a** was identified as a potent PTP1B inhibitor (IC_{50} = 0.86 μM) with 5-fold selectivity over the highly homologous TCPTP. Long-term oral administration of **5a** at a dose of 50 mg/kg not only significantly reduced blood glucose levels, triglycerides (TG) and low-density lipoprotein cholesterol (LDL-C) levels but also ameliorated insulin sensitivity in diabetic BKS db mice. Moreover, **5a** enhanced the insulin-stimulated phosphorylation of IRβ, IRS-1 and Akt in C2C12 myotubes. A histopathological evaluation of liver and pancreas demonstrated that **5a** increased liver glycogen storage and improved islet architecture with more β-cells and fewer α-cells in diabetic mice. Thus, our work demonstrated that compound **5a** could serve as a lead compound for the discovery of new antidiabetic drugs.

1. Introduction

Type 2 diabetes mellitus (T2DM) is a complex endocrine and metabolic disease, which is characterized by insulin resistance and progressive β-cell dysfunction. Owing to the sedentary lifestyle and obesity in the population, T2DM is now a major public health problem worldwide. According to the latest Diabetes Atlas (9th edition 2019) published by International Diabetes Federation (IDF), 463 million people (20–79 years) had diabetes in 2019, and this number is estimated to exceed 700 million globally by 2045 [1]. In China, the problem is particularly overwhelming, with 116 million adults considered to have T2DM in 2019, which ranked first in the world. These staggering data document the increasing incidence of T2DM and strongly indicate the medical need for new and better agents to treat this disease.

Protein tyrosine phosphatase 1B (PTP1B) was the first mammalian protein tyrosine phosphatase (PTP) to be isolated and characterized from human placenta [2]. The significance of PTP1B is that it plays crucial roles in regulating the intracellular phosphorylation of proteins. A series of biochemical, cellular and knockout mouse studies have demonstrated that PTP1B is a key negative regulator of both insulin and leptin signaling pathways [3–6]. Thus, PTP1B has become an attractive therapeutic target for T2DM treatment. Additionally, accumulating evidence suggests that PTP1B also plays an increasingly important role in other human diseases such as breast cancer [7], hepatocellular carcinoma [8] and nonalcoholic fatty liver disease [9].

In light of convincing evidence that PTP1B is related to many human diseases, the development of small-molecule PTP1B inhibitors has attracted considerable attention in both fundamental research and pharmaceutical industries. To date, only two small-molecule PTP1B inhibitors, ertiprotafib [10] and trodusquemine [11] (Fig. 1), have reached clinical trials, but the studies were discontinued due to poor clinical efficacy and undesirable side effects. A first-in-class drug has yet to be launched; nevertheless, extensive research is underway to develop a potential drug candidate. Over the past decades, various compounds

* Corresponding author at: Key Laboratory of Experimental Marine Biology, Institute of Oceanology, Chinese Academy of Sciences, Qingdao 266071, China.
E-mail address: wanglijun@qdio.ac.cn (L. Wang).
[1] These authors contributed equally to this work.

https://doi.org/10.1016/j.bioorg.2021.104648
Received 15 June 2020; Received in revised form 15 November 2020; Accepted 6 January 2021
Available online 12 January 2021

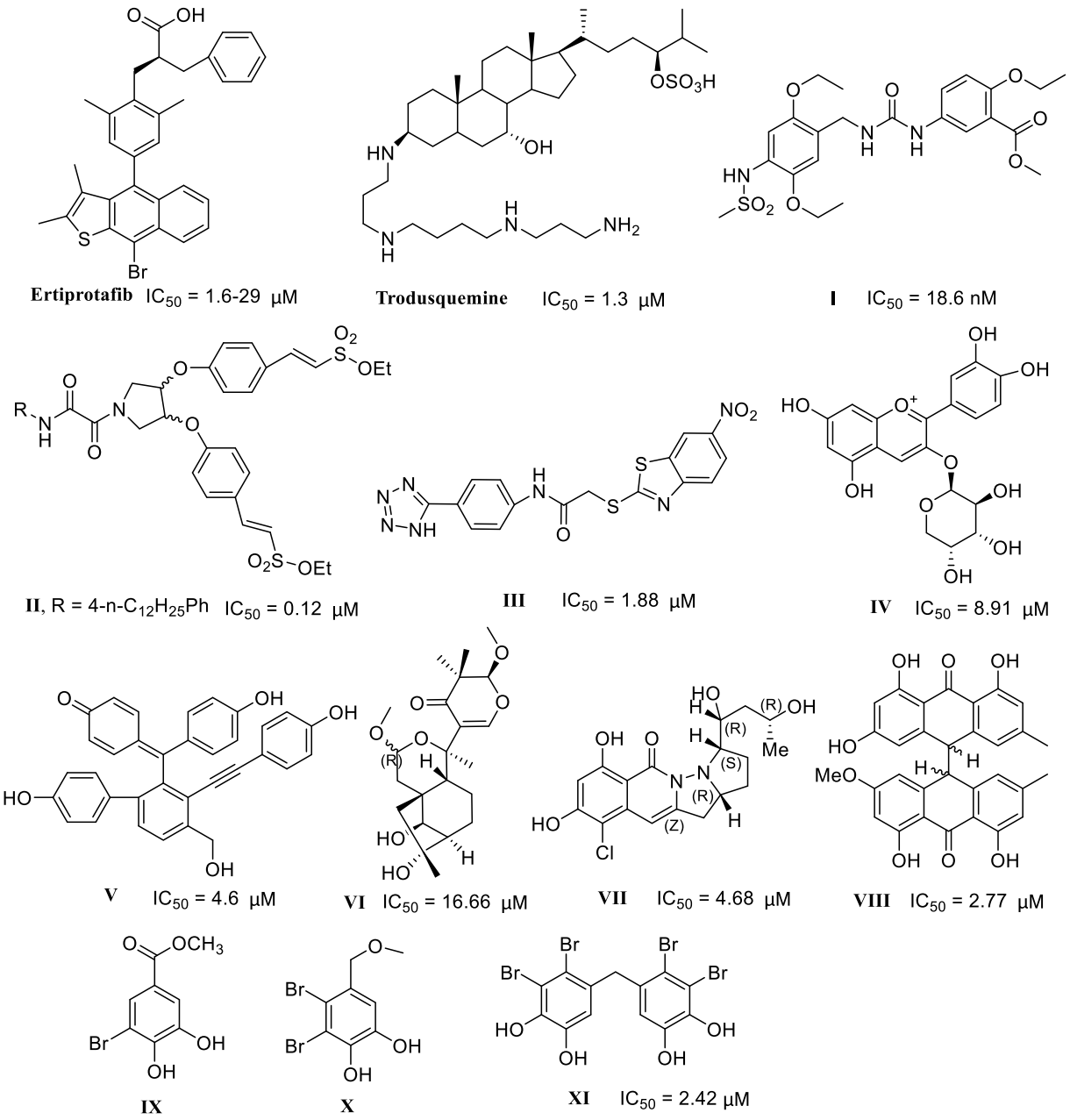

Fig. 1. Representative examples of PTP1B inhibitors I-VIII and bromophenol compounds IX-XI isolated from red alga.

containing negatively charged non-hydrolyzable pTyr mimetics have been reported to exhibit excellent potency (at nanomolar range) *in vitro* [12,13]; however, the low cell permeability and bioavailability of these compounds have limited their application for the development of effective drugs. Therefore, less acidic molecules may provide alternatives in developing less potent PTP1B inhibitors with improved cell permeability and bioavailability.

Recent studies have reported that small molecules with good enzyme inhibition and devoid of negatively charged groups (compounds **I-III**, as shown in Fig. 1) are highly desirable for the discovery of PTP1B inhibitors [14–16]. In addition, natural products are abundant sources of bioactive molecules. Intriguingly, several natural products have been found to have PTP1B inhibitory activity through their unique scaffolds, instead of relying on the functionalities of mimicking pTyr. Fig. 1 displays some representative PTP1B inhibitors (compounds **IV-VIII**) isolated from natural plants with IC_{50} values of moderate to good potency [17–21].

Compounds bearing a 2,4-thiazolidinedione (TZD) moiety were shown to exhibit various biological effects, including anti-inflammatory [22], antidiabetic [23], antibacterial [24] and anti-Alzheimer's disease effects [25]. In particular, TZDs, known as high-affinity PPARγ agonists, were introduced in the late 1990s as the first agents for the treatment of type 2 diabetes [26]. Additionally, hydantoin, the bioisostere of TZD, represent a kind of new and less acidic pTyr mimetic that can be used for the development of potent PTP1B inhibitors. Our group has long been engaged in isolation of bromophenol compounds from marine algae [27]. Fig. 1 shows partial structures of mono-benzyl and di-benzyl bromophenols and some of them exhibited potent PTP1B inhibition (compounds **IX-XI**) [28]. Considering these findings, TZDs and hydantoin were introduced on the bromophenols scaffold to obtain potent PTP1B inhibitors lacking negatively charged pTyr mimetic. The antidiabetic activities both *in vitro* and *in vivo* as PTP1B inhibitors along with mechanistic studies were further investigated.

2. Chemistry

The TZD derivatives **1a-g** and hydantoin derivatives **2a-e** were synthesized according to the general procedures depicted in Schemes 1 and 2. Knoevenagel condensation of appropriate benzaldehydes with TZD or hydantoin in the presence of ammonium acetate generated the corresponding arylidenes **1a-g** and **2a-e** in good yields. The compounds **5a-b** and **8a-b** were synthesized as described inFig. Scheme 3. The key intermediates **3** and **6** were obtained via well documented procedures [28]. Oxidation of benzyl alcohol (**3**) using pyridinium chlorochromate (PCC) as an oxidant afforded aryl aldehyde **4** in good yield. Alkylation of 4-hydroxy benzaldehyde with benzyl bromide (**6**) in the presence of potassium carbonate in acetone gave the corresponding aryl aldehyde **7**. Similarly, the Knoevenagel reaction of **4** or **7** with TZD in acetic acid as the solvent afforded the target compounds **5a** and **8a**, respectively. Finally, the olefinic bond of the 5-arylidene-2,4-thiazolidinediones **5a** and **8a** was reduced with hydrogen in methanol using 10% palladium on carbon as the catalyst to give compounds **5b** and **8b**, respectively.

The ^{1}H NMR spectra of the 5-arylidene-2,4-thiazolidinediones **1a-g**, **5a** and **8a** showed a singlet for exocyclic olefinic protons at 7.63–7.86 ppm in DMSO-d_6 solution, suggesting that these compounds were assigned to the *Z*-configuration. In the case of Knoevenagel condensation between *N*1-unsubstituted hydantoin and the corresponding benzaldehydes, the *Z*-configuration was also preferable for the hydantoin derivatives **2a-e** [29]. Furthermore, the *Z*-configuration has been considered thermodynamically more stable than the *E*-configuration on the basis of literature data for similar compounds [30,31].

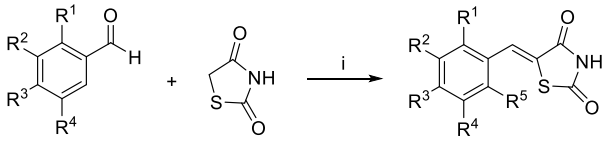

Compd	R^1	R^2	R^3	R^4	R^5
1a	H	OCH_3	OH	H	H
1b	H	OCH_3	OH	Br	H
1c	H	OCH_3	OCH_3	Br	H
1d	H	OCH_3	OCH_3	Br	Br
1e	H	OH	OH	Br	H
1f	Br	OCH_3	OCH_3	H	H
1g	H	OCH_3	OH	Br	Br

Scheme 1. Synthesis of TZD derivatives 1a-g. Reagents and conditions: (i) 3 equiv NH_4OAc, AcOH, reflux, 24 h.

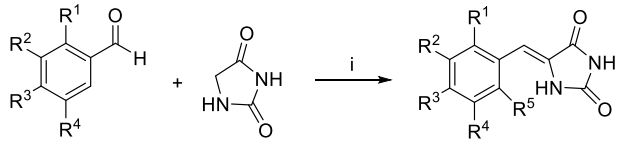

Compd	R^1	R^2	R^3	R^4	R^5
2a	H	OCH_3	OCH_3	Br	H
2b	Br	OCH_3	OCH_3	H	H
2c	H	OCH_3	OH	H	H
2d	H	OCH_3	OH	Br	H
2e	H	OCH_3	OH	Br	Br

Scheme 2. Synthesis of hydantoin derivatives 2a-e. Reagents and conditions: (i) 3 equiv NH_4OAc, AcOH, reflux, 24 h.

3. Results and discussion

3.1. PTP1B inhibitory activities and structure–activity relationship

The *in vitro* inhibitory activities of compounds **1a-g**, **2a-e**, **5a-b** and **8a-b** were tested against recombinant human PTP1B. First, we measured the percentage inhibitory rates of all the synthetic compounds at 20 μg/mL. Compounds with inhibition rates >50% were selected for further determination of IC_{50} values. As summarized in Table 1, all the hydantoin derivatives exhibited low inhibitory rates, indicating that the hydantoin was not tolerated. The TZD compounds bearing a mono-aryl ring offered slightly better activity than the hydantoin ones. Two of them (**1d** and **1e**) displayed moderate potency (8.34 ± 1.75 and 10.51 ± 2.55 μM, respectively). Although the mono-aryl ring compounds did not offer acceptable efficacy, it was encouraging to note that the diaryl-methane scaffold with substitutions of bromines was crucial for better inhibitory activity against PTP1B (Table 2). Comparing with those of previously reported diaryl-methane derivatives **XII-XIV**, compounds **5a-b** and **8a-b** showed improved potency with an IC_{50} range from moderate to potent (0.86–12.77 μM), thus confirming the favorable role of the diaryl-methane bearing TZD moiety in enhancing inhibition against the target enzyme. Furthermore, the number of bromine substitution on the aryl ring had a certain influence on the inhibitory activity. Especially the tri-brominated compounds (**5a-b** and **8a-b**) and di-brominated compounds (**1d**) displayed more significant PTP1B inhibitory activity than mono-brominated or non-brominated compounds. It is also found that the reduction of the olefinic bond of **5a** was less sensitive to modifications. On the contrary, the reduction of **8a** led to **8b** with improved potency (12.77 ± 6.08 and 2.10 ± 0.23 μM, respectively). Among them, compound **5a** was the most active, with a submicromolar IC_{50} of 0.86 ± 0.29 μM.

3.2. Selectivity, kinetics and docking studies of compound *5a*

Although PTP1B has been identified as a validated target for T2DM, the development of a selective PTP1B inhibitor remains a challenging task because the closest homologue of PTP1B, TCPTP, shares 74% sequence identity in the catalytic domain. Therefore, the selectivity issue for PTP1B is critically important [32]. In addition to good PTP1B inhibition, compound **5a** was selected for testing against a panel of PTPs, including TCPTP, SHP-1, SHP-2 and LAR. As shown in Fig. 2A, compound **5a** showed 5-fold selectivity against TCPTP. Furthermore, **5a** demonstrated excellent selectivity against SHP-1, SHP-2 and LAR (>20-fold).

Kinetics analysis was conducted to elucidate the mode of inhibition of compound **5a**. A series of concentrations of **5a** (1.0, 2.0, 4.0, 8.0 μM) and the substrate pNPP (0.5, 1.0, 2.0, 4.0 and 8 mM) were used in this assay. Fig. 2B shows the Lineweaver-Burk plots for inhibition. Various concentration lines of compound **5a** intersected in the second quadrant, indicating that **5a** inhibited PTP1B in a mixed manner. When the inhibitor concentration was increased, the increased Km values and reduced Vmax values confirmed **5a** as a mixed inhibition of PTP1B (Fig. 2C and D).

Molecular docking was conducted to investigate the binding interactions of compound **5a** with the PTP1B active sites (PDB code 1G1H). As shown in Fig. 2E and F, the aryl ring bearing TZD moiety oriented itself to the pocket, which was surrounded by the WPD loop, the Q loop, and the pTyr loop. The oxygen atom of thiazolidinedione formed two hydrogen bonds with Arg 221. Another single hydrogen bond interaction was observed between the oxygen atom on the methoxy group of **5a** and Lys 120. The phenyl ring was sandwiched between the aromatic side chains of Tyr 46 and Phe 182, which provided

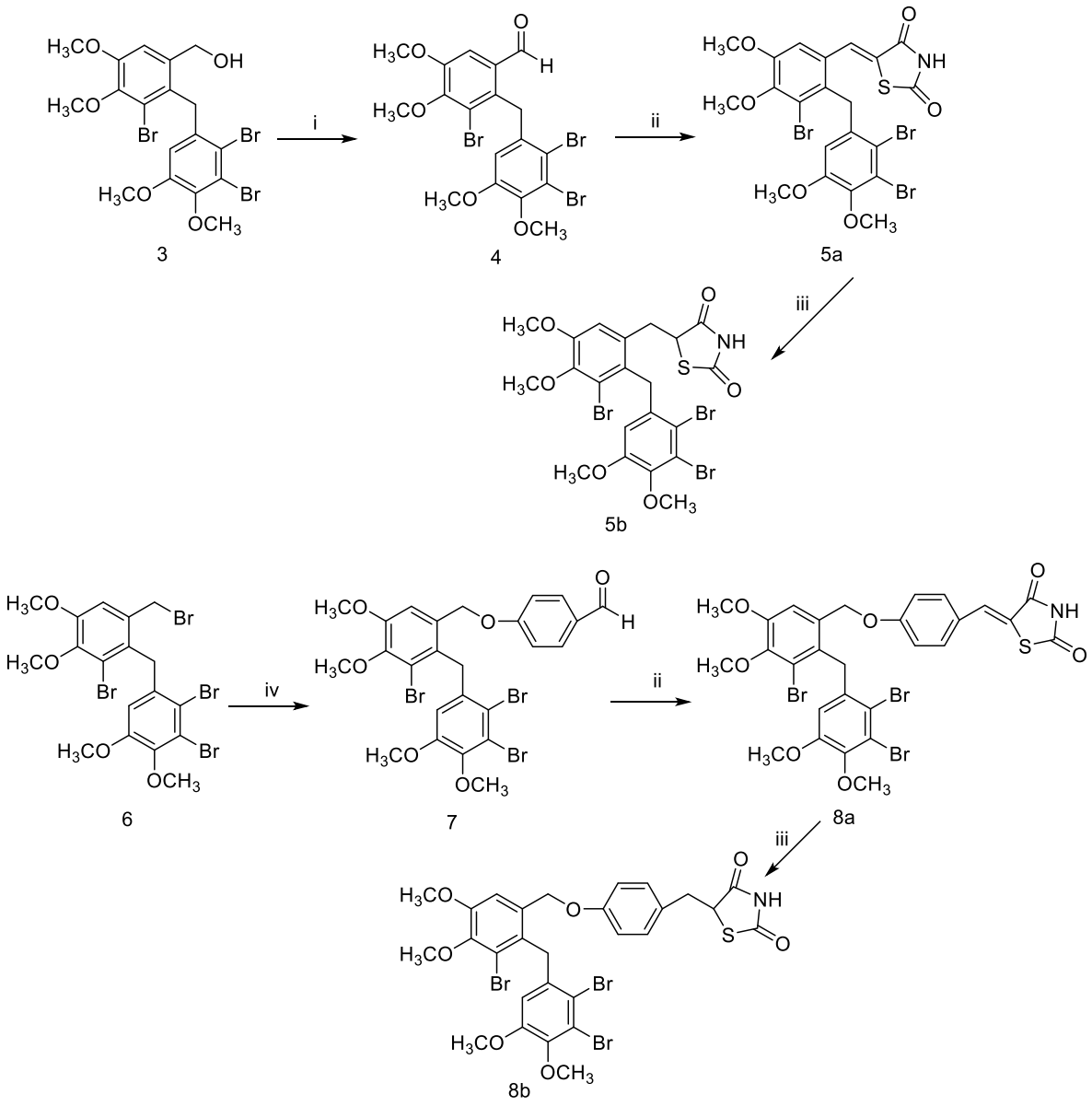

Scheme 3. Synthesis of TZD derivatives 5a-b and 8a-b. Reagents and conditions: (i) 2 equiv pyridinium chlorochromate, dry CH_2Cl_2, room temperature, 2 h; (ii) 1.2 equiv TZD, 3 equiv NH_4OAc, AcOH, reflux, 24 h; (iii) H_2, 10% Pd/C, MeOH, 50 °C, 5 h; (iv) 1.2 equiv 4-ydroxybenzaldehyde, K_2CO_3, acetone, room temperature, overnight.

a π–π stacking interaction. The second aryl ring of **5a** extended out of the pocket.

3.3. Cellular activities of compound *5a*

Firstly, the cell permeability of compound **5a** was analyzed by HPLC in C2C12 myotubes. The result showed that the proportion of **5a** in the cell lysate was about 61.43% (Fig. 3A–C), indicating that **5a** successfully crossed the plasma membrane and accumulated intracellularly.

We next examined the cytotoxicity on C2C12 myotubes treated with various concentrations of compound **5a**, and cell viability was measured by CCK8 assay. As shown inFig. 3D, up to 25 μM treatment with compound **5a** for 24 h did not reduce the survival of C2C12 cells. When concentration reached to 100 μM, the cell viability lose 50%. Accordingly, further *in vitro* studies on the insulin signaling activation of **5a** were conducted in the range of 0.01–10 μM.

The phosphorylation cascade of IRβ, IRS1, and Akt is an indicator of insulin pathway activation [33]. To determine whether compound **5a** could affect insulin signaling, we treated C2C12 skeletal muscle cells with a series of concentrations of compound **5a** (ranging from 0.01 to 10 μM) with/without insulin stimulation. Notably, compound **5a** treatment increased the insulin-stimulated phosphorylation of IRβ Y1158 and IRS1Y608 (Fig. 3D-E). Moreover, the phosphorylation level of Akt on Ser473 also increased after compound **5a** treatment. Moreover, the insulin-sensitizing effect of compound **5a** was dose-depend at concentrations between 0.1 and 10 μM. Furthermore, the expression level of PTP1B protein was also examined by immunoblotting, and the results showed that it was not changed by intervention of compound **5a**. These results demonstrate that compound **5a**, a potent PTP1B inhibitor, enhances insulin-stimulated signaling without affecting PTP1B protein levels.

3.4. In vivo anti-diabetic activity assays

3.4.1. Hypoglycemic effect of compound *5a*

The *in vivo* efficacy of many PTP1B inhibitors is inconsistent with

Table 1
In vitro PTP1B inhibitory activities of compounds **1a-g** and **2a-e.**

Compds	Inhibition (%) at 20 μg/mL	IC_{50} (μM)[a]
1a	13.34	ND[b]
1b	47.51	ND
1c	39.87	ND
1d	95.95	8.34 ± 1.75
1e	98.82	10.51 ± 2.55
1f	14.94	ND
1g	35.22	ND
2a	12.08	ND
2b	19.78	ND
2c	28.67	ND
2d	32.20	ND
2e	31.38	ND
Oleanolic acid		2.04 ± 0.11

[a] Values are expressed as means ± standard deviations. All tests were performed in triplicate.
[b] ND = not determined, inhibition rate < 50% at 20 μg/mL was not determined.

Table 2
In vitro PTP1B inhibitory activities of compounds **5a-b** and **8a-b,** in comparison with previous analogues **XII-XIV**.

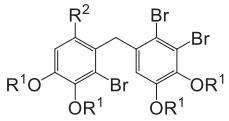

Compds	R^1	R^2	Inhibition (%) at 20 μg/mL	IC_{50} (μM)[a]
5a	CH_3		95.72	0.86 ± 0.29
5b	CH_3		67.90	1.84 ± 0.40
8a	CH_3	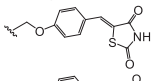	93.39	12.77 ± 6.08
8b	CH_3	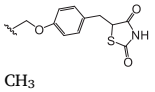	94.27	2.10 ± 0.23
XII	CH_3	CH_3	87.52	ND[b,c]
XIII	CH_3	CH_2OH	74.86	ND[b,c]
XIII	H	$CH_2O(CH_2)_2CH_3$	86.15	2.00[c]
XIV	H	$CH_2OCH_2CH(CH_3)_2$	96.25	1.50[c]

[a] Values are expressed as means ± standard deviations. All tests were performed in triplicate.
[b] ND = not determined, inhibition rate <50% at 5 μg/mL was not determined.
[c] Ref. [28].

their observed *in vitro* activities. Thus, we used a spontaneous diabetic mouse model, BKS db mice, to evaluate the antidiabetic effects of compound **5a**. The first-line T2DM drug, metformin, was used as the positive control. As shown in Fig. 4A, compound **5a** showed a marked trend towards a decrease in blood glucose levels compared with the vehicle-treated diabetic mice. **5a** significantly lowered the blood glucose levels of BKS db mice from the 3rd week ($p < 0.01$) and lasted for the 5th week. Moreover, the plasma glycosylated serum protein (GSP) levels were significantly reduced by compound **5a** ($p < 0.01$) (Fig. 4B).

We next examined the effect of compound **5a** on insulin sensitivity using the ITT assay in diabetic BKS db mice. As shown in Fig. 4C, compound **5a** notably suppressed blood glucose levels in diabetic mice after insulin injection for 30 min ($p < 0.05$), 60 min ($p < 0.01$), and 120 min ($p < 0.001$). These results indicated that insulin sensitivity had been ameliorated in diabetic mice treated with compound **5a**.

Furthermore, a simplified OGTT experiment was used to evaluate the effect of compound **5a** on glucose tolerance in diabetic mice. As shown in Fig. 4D, 2 h after of glucose administration, the blood glucose levels of compound **5a**-treated diabetic mice were significantly lower than the vehicle-treated diabetic mice, suggesting that compound **5a** administration improved glucose tolerance in diabetic mice.

3.4.2. *Effects of compound **5a** on dyslipidemia*

T2DM is usually accompanied by dyslipidemia, which is characterized by elevated total cholesterol (TC) and triglyceride (TG) and reduced high-density lipoprotein-cholesterol (HDL-C) levels [34]. Thus, we further examined whether compound **5a** could improve serum lipid dysregulation in diabetic mice. As shown in Fig. 5A and C, compound **5a** significantly reduced TG and LDL-C levels in diabetic BKS db mice compared with the vehicle treatment group. Compound **5a** also effectively suppressed circulating free fatty acid (FFA) levels (Fig. 5E). However, it had no effect on blood TC and HDL-C levels (Fig. 5B and D). These results suggested that compound **5a** could ameliorate dyslipidemia in diabetic mice.

3.4.3. *Effects of compound **5a** on water intake, food intake and body weight*

Polyphagia, polyuria and obesity are typical characteristics of T2DM patients. Next, we tested the effects of compound **5a** on water intake, food intake, and body weight in BKS db mice. At baseline, there was no difference in water intake, food intake, or body weight among all diabetic mice. Compound **5a** treatment significantly reduced water intake in diabetic mice during the intervention compared with vehicle treatment (Fig. 6A). However, both compound **5a** and metformin had no effect on food intake and body weight of diabetic mice (Fig. 6B and C). In contrast, compound **5a** effectively blocked the increased ratio of abdominal fat (Fig. 6D).

3.4.4. *Oral administration of compound **5a** increased Akt phosphorylation in skeletal muscle tissues of diabetic mice*

Given that phosphorylation of Akt Ser473 is a key event in glucose metabolism [35], Akt phosphorylation of skeletal muscle tissues treated with/without compound **5a** was detected. Western blotting results showed that diabetic mice treated with compound **5a** exhibited increased phosphorylation levels of Akt at serine 473 (Fig. 7).

3.4.5. *Histological analysis of the liver*

Impaired glycogen storage is observed in T2DM patients [36]. To investigate the effect of compound **5a** on diabetic mice liver, we performed H&E and PAS staining of liver sections. As shown in Fig. 8, the liver of vehicle-treated diabetic mice exhibited markedly vacuolated and swollen hepatocytes, and these vacuolated hepatocytes were significantly reduced in the liver of compound **5a**-treated mice. PAS staining was used to detect hepatic glycogen, and severe glycogen depletion was found in diabetic mice compared with normal BKS mice. However, this depletion could be reversed by compound **5a** treatment, suggesting that compound **5a** promoted liver glycogen storage in diabetic mice.

3.4.6. *Histological analysis of the pancreas*

To investigate the beneficial effect of compound **5a** on the pancreas, a series of histological staining analyses were performed. Glucagon-positive staining showed pancreatic α-cells distributed on the edge of islets in normal control mice, while islets in diabetic mice contained more α-cells, which were scattered throughout the entire islet (Fig. 9). Compound **5a** could reduce the number of α-cells in islets in diabetic mice. Insulin-positive cells were markedly decreased compared with normal BKS mice, indicating a reduced number of β-cells in diabetic mice. Compound **5a** increased the number of insulin-positive cells, suggesting the presence of more β-cells in the islets of compound **5a**-treated mice. The same results were observed for glucagon-positive and insulin-positive double-staining.

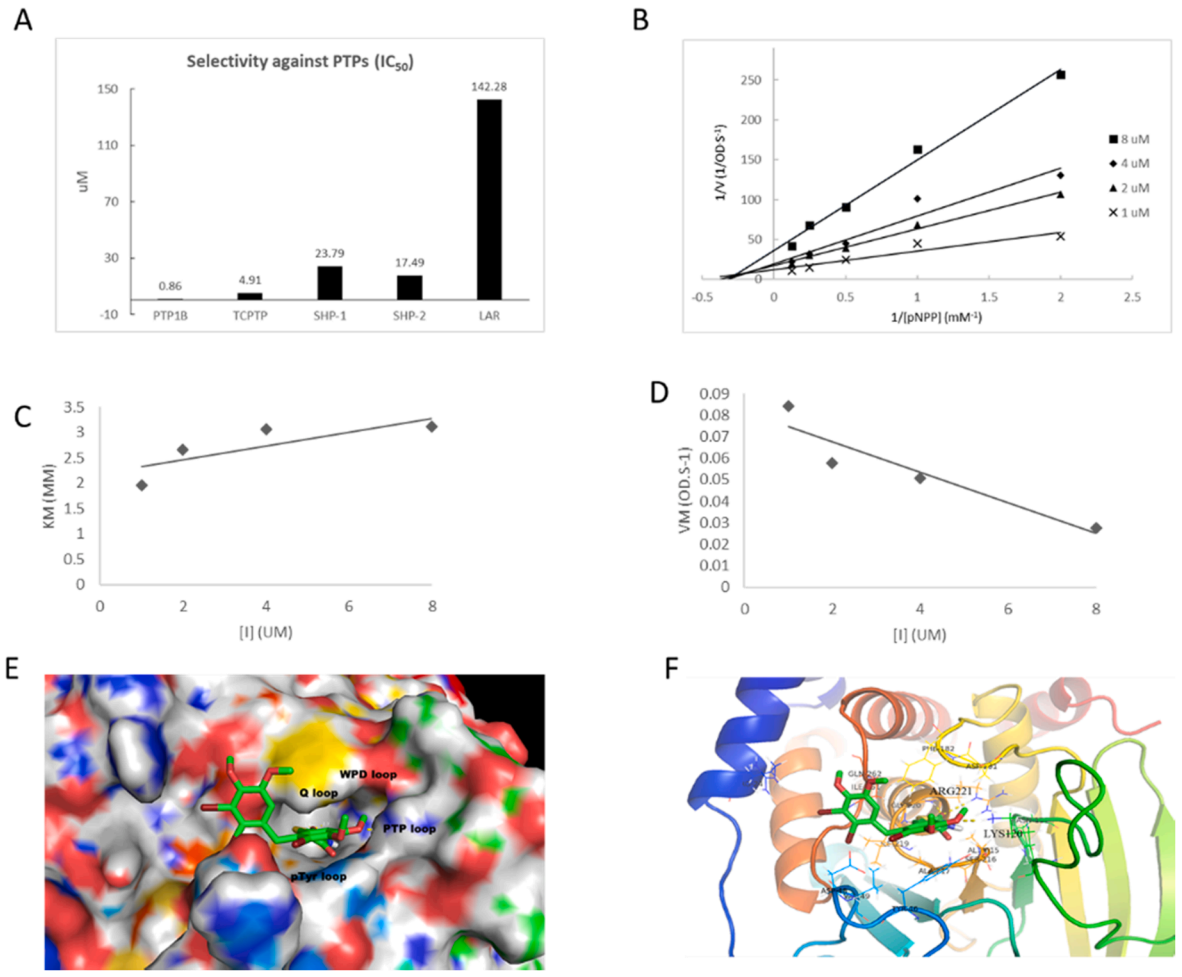

Fig. 2. Selectivity, kinetic and docking studies of compound **5a**. (A) Selectivity of compound **5a** against other PTPs. (B) The Lineweaver-Burk plot for inhibition of PTP1B enzyme reaction by compound **5a**. Concentrations of **5a** were 1 (×), 2 (▲), 4 (◆) and 8 μM (■), respectively. (C) The plot of apparent Km *versus* the concentrations of compound **5a**. (D) The plot of Vmax *versus* the concentrations of compound **5a**. (E) Surface representation of PTP1B in Complex with compound **5a**. (F) Binding mode of compound 5a in the active site of PTP1B. Carbon is in green for compound **5a**, oxygen is in red, nitrogen is in blue, sulfur is in yellow. Hydrogen bonds were considered within 2.5 Å and represented as yellow dots. (For interpretation of the references to color in this figure legend, the reader is referred to the web version of this article.)

4. Conclusions

In summary, we have prepared a series of TZD and hydantoin derivatives to search for selective PTP1B inhibitors with good cell permeability and oral bioavailability. The preliminary structure–activity relationship indicated that the TZD bearing the diaryl-methane scaffold with substitutions of bromines had favorable PTP1B inhibitory activity. Among these derivatives, compound **5a** exhibited potent inhibitory activity against PTP1B and high selectivity against other PTPs. More importantly, compound **5a** effectively lowered glucose, TG and LDL-C levels in a db/db mouse model at 50 mg/kg. The novel 5-benzylidene-thiazolidine-2,4-dione reported in this study could provide a possible lead compound for the development of selective PTP1B inhibitors with improved pharmacological properties.

5. Experimental

5.1. Chemistry

5.1.1. General

All the reagents and solvents were purchased from commercial sources and used without further purification. Reactions were monitored by analytical thin layer chromatography (TLC) performed on silica gel GF254 precoated plates and visualized with a UV lamp (254 nm) or 95% $FeCl_3$-EtOH solution. Column chromatography was carried out using silica gel (200–300 mesh). Melting points (mp) were determined using a Boetius electrothermal capillary melting point apparatus and were uncorrected. ^{1}H NMR and ^{13}C NMR spectra were recorded on an Inova (500 MHz) NMR spectrometer for protons and 125 MHz for carbon. Deuterated dimethyl sulfoxide (DMSO) was used as a solvent. Chemical shifts are reported in ppm (δ) relative to tetramethylsilane (TMS) as an internal standard. Multiplicities are presented as s (singlet), d (doublet), m (multiplet) and br s (broad signal). Coupling constants (J values) are given in hertz (Hz). The acidic protons of the amidic –NH in the thiazolidindione ring and phenolic hydroxyl were not frequently observed in ^{1}H NMR spectra. High-resolution mass spectral (HRMS) data were obtained using a Thermo LTQ-Orbitrap mass spectrometer.

5.1.2. General procedure for the synthesis of TZD derivatives ***1a-g***

To a stirred suspension of the appropriate benzaldehyde (1 equiv) in AcOH (20 mL) was sequentially added 2,4-thiazolidinedione (1.2 equiv) and NH_4OAc (3 equiv). After refluxing for 24 h, the reaction mixture was cooled and then poured into H_2O. In the event that a precipitate was formed, the suspension was filtered, and the residue was washed with cold water. The washed residue was dried to obtain the desired derivatives of 5-benzylidenethiazolidine-2,4-dione as yellow residues.

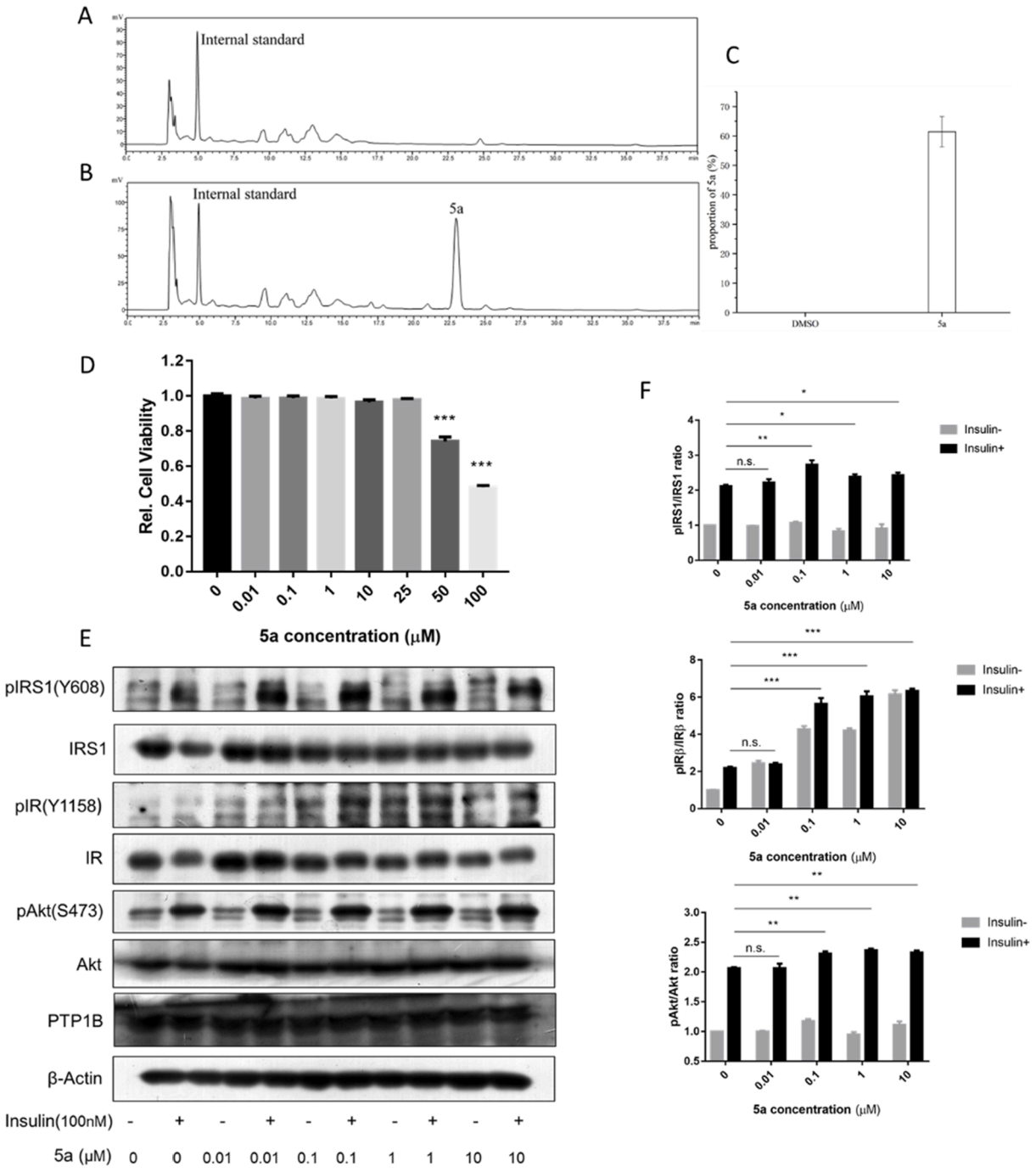

Fig. 3. Compound **5a** increases insulin signaling activity after insulin stimulation. (A-C) Cell permeability of **5a** in C2C12 myotubes. (A) HPLC analysis of DMSO-treated group (control). (B) HPLC analysis of 5a-treated group. C2C12 myotubes were treated with **5a** (10 μM) for 8 h in a 10 cm cell plate. (C) Uptake ratio of 5a in C2C12 myotubes. (D) Cytotoxicity of **5a** to C2C12 myotubes. Cells were incubated with **5a** for 24 h, and cells viability was determined by CCK8 method. The data was expressed as the mean ± SEM (n = 6), ***$p < 0.001$ *versus* control group. (E) Enhanced insulin signaling in C2C12 myotubes treated with compound **5a**. Serum starved C2C12 myotubes were treated with compound **5a** for 8 h and then exposed with/without 100 nM insulin for 5 min. Cells was then lysed and immunoblotting was performed to detect IRS1/IRβ/Akt phosphorylation and PTP1B protein. (F) Relative ratio of pIRS-1/IRS-1, pIRβ/IRβ and pAkt/Akt. Data are expressed as mean ± SEM (n = 3). * $p < 0.05$, ** $p < 0.01$, and *** $p < 0.001$, as indicated.

However, in the absence of precipitation, the mixture was extracted with EtOAc (2x), washed successively with saturated $NaHCO_3$ solution and brine, dried over anhydrous Na_2SO_4, and concentrated in vacuo. The residue was purified by silica gel column chromatography to afford the target compounds as a yellowish solid.

*5.1.2.1. (Z)-5-(4-hydroxy-3-methoxybenzylidene)thiazolidine-2,4-dione (**1a**).* Yellow solid, Yield 70%, mp: 230–232 °C, ^{1}H NMR (500 MHz, DMSO-d_6) δ: 3.82 (s, 3H), 6.93 (d, $J = 8.25$ Hz, 1H), 7.07 (d, $J = 8.25$ Hz, 1H), 7.16 (s, 1H), 7.71 (s, 1H), 9.93 (br s, 1H), 12.56 (br s, 1H); ^{13}C NMR (125 MHz, DMSO-d_6) δ: 55.63, 114.21, 116.13, 119.22, 124.41, 132.56, 147.90, 149.45, 167.38, 167.96; HRESIMS: calc for C11H8NO4S $[M-H]^-$ 250.0180, found 250.0178.

*5.1.2.2. (Z)-5-(3-bromo-4-hydroxy-5-methoxybenzylidene)thiazolidine-2,4-dione (**1b**).* Yellow solid, Yield 73%, mp: 251–253 °C, ^{1}H NMR (500

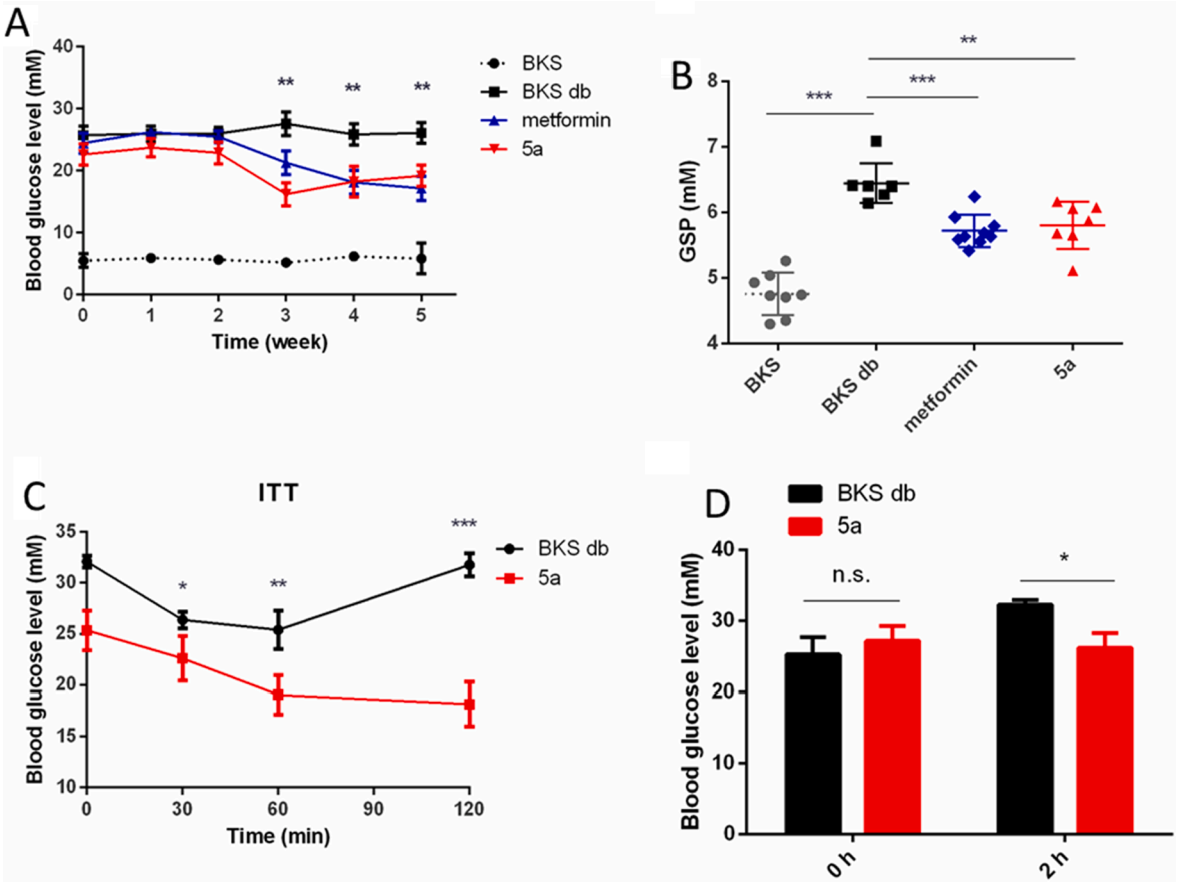

Fig. 4. Hypoglycemic effects of compound **5a** in diabetic BKS db mice. Mice were treated with vehicle, compound **5a** (50 mg/kg/day), or metformin (100 mg/kg/day) by oral gavage. (A) Blood glucose levels of diabetic mice treated with vehicle, compound **5a**, or metformin and of normal BKS mice treated with vehicle after 6 h fasting. (B) GSP levels of all the groups of mice. (C) Effects of compound **5a** on insulin resistance in diabetic mice. (D) Blood glucose levels in vehicle- and compound **5a**-treatment group 2 h after glucose administration. Data were shown as means ± SEM (n = 6–8). *$p < 0.05$, **$p < 0.01$, and ***$p < 0.001$, compound **5a**-treatment group *versus* vehicle-treated diabetic mice, or as indicated.

MHz, DMSO-d_6) δ: 3.88 (s, 3H), 7.17 (s, 1H), 7.35 (s, 1H), 7.69 (s, 1H), 10.42 (br s, 1H), 12.61 (br s, 1H); ^{13}C NMR (125 MHz, DMSO-d_6) δ: 56.3, 109.8, 112.4, 121.2, 125.3, 126.8, 131.1, 146.2, 148.5, 167.2, 167.6; HRESIMS: calc for C11H7BrNO4S $[M-H]^-$ 327.9285, found 327.9282.

5.1.2.3. (Z)-5-(3-bromo-4,5-dimethoxybenzylidene)thiazolidine-2,4-dione ***(1c)***. Yellow solid, Yield 70%, mp: 216–218 °C, ^{1}H NMR (500 MHz, DMSO-d_6) δ: 3.79 (s, 3H), 3.88 (s, 3H), 7.26 (s, 1H), 7.39 (s, 1H), 7.73 (s, 1H), 12.66 (br s, 1H); ^{13}C NMR (125 MHz, DMSO-d_6) δ: 56.81, 60.88, 114.33, 117.84, 124.61, 126.37, 130.94, 131.08, 147.43, 153.95, 167.69, 168.09; HRESIMS: calc for C12H9BrNO4S $[M-H]^-$ 341.9441, found 341.9440.

5.1.2.4. (Z)-5-(2,3-dibromo-4,5-dimethoxybenzylidene)thiazolidine-2,4-dione ***(1d)***. Yellow solid, Yield 75%, mp: 283–285 °C, ^{1}H NMR (500 MHz, DMSO-d_6) δ: 3.81 (s, 3H), 3.89 (s, 3H), 7.18 (s, 1H), 7.81 (s, 1H), 12.60 (br s, 1H); ^{13}C NMR (125 MHz, DMSO-d_6) δ: 56.44, 60.40, 111.96, 118.29, 121.97, 127.88, 130.53, 130.58, 148.17, 152.40, 166.68, 167.47; HRESIMS: calc for C12H8BrNO4S $[M-H]^-$ 421.8526, found 421.8522.

5.1.2.5. (Z)-5-(3-bromo-4,5-dihydroxybenzylidene)thiazolidine-2,4-dione ***(1e)***. Yellow solid, Yield 72%, mp: 276–278 °C, ^{1}H NMR (500 MHz, DMSO-d_6) δ: 7.01 (s, 1H), 7.28 (s, 1H), 7.59 (s, 1H); ^{13}C NMR (125 MHz, DMSO-d_6) δ:110.64, 114.93, 121.25, 125.72, 127.39, 131.75, 146.27, 147.07, 168.03, 168.50; HRESIMS: calc for C10H5BrNO4S $[M-H]^-$ 313.9128, found 313.9132.

5.1.2.6. (Z)-5-(2-bromo-3,4-dimethoxybenzylidene)thiazolidine-2,4-dione ***(1f)***. Yellow solid, Yield 91%, mp:198–200 °C, ^{1}H NMR (500 MHz, DMSO-d_6) δ: 3.75 (s, 3H), 3.89 (s, 3H), 7.24 (d, J = 7.5 Hz, 1H), 7.31 (d, J = 7.5 Hz, 1H), 7.79 (s, 1H); ^{13}C NMR (125 MHz, DMSO-d_6) δ: 56.56, 60.43, 112.91, 121.52, 125.15, 125.45, 126.52, 127.68, 146.93, 154.96, 169.64, 171.21; HRESIMS: calc for C12H9BrNO4S $[M-H]^-$ 341.9441, found 341.9445.

5.1.2.7. (Z)-5-(2,3-dibromo-4-hydroxy-5-methoxybenzylidene)thiazolidine-2,4-dione ***(1g)***. Yellow solid, Yield 72%, mp:198–200 °C, ^{1}H NMR (500 MHz, DMSO-d_6) δ: 3.88 (s, 3H), 7.04 (s, 1H), 7.86 (s, 1H), 10.81 (br s, 1H), 12.70 (br s, 1H); ^{13}C NMR (125 MHz, DMSO-d_6) δ: 56.95, 110.76, 114.85, 120.59, 125.21, 125.61, 131.81, 147.85, 147.91, 167.52, 168.27; HRESIMS: calc for C11H6Br2NO4S $[M-H]^-$ 405.8390, found 405.8391.

5.1.3. General procedure for the synthesis of hydantoin derivatives ***2a-e***

As described in procedure 5.1.2.

5.1.3.1. (Z)-5-(3-bromo-4,5-dimethoxybenzylidene)imidazolidine-2,4-dione ***(2a)***. Yellow solid, Yield 86%, mp: 280–282 °C, ^{1}H NMR (500 MHz, DMSO-d_6) δ: 3.75 (s, 3H), 3.89 (s, 3H), 6.35 (s, 1H), 7.20 (s, 1H), 7.46 (s, 1H), 10.76 (br s, 1H), 11.28 (br s, 1H); ^{13}C NMR (125 MHz, DMSO-d_6) δ: 56.82, 60.71, 107.15, 114.10, 117.55, 125.59, 128.26, 130.95, 145.91, 153.94, 156.64, 166.24; HRESIMS: calc for C12H10BrN2O4 $[M-H]^-$ 324.9829, found 324.9823.

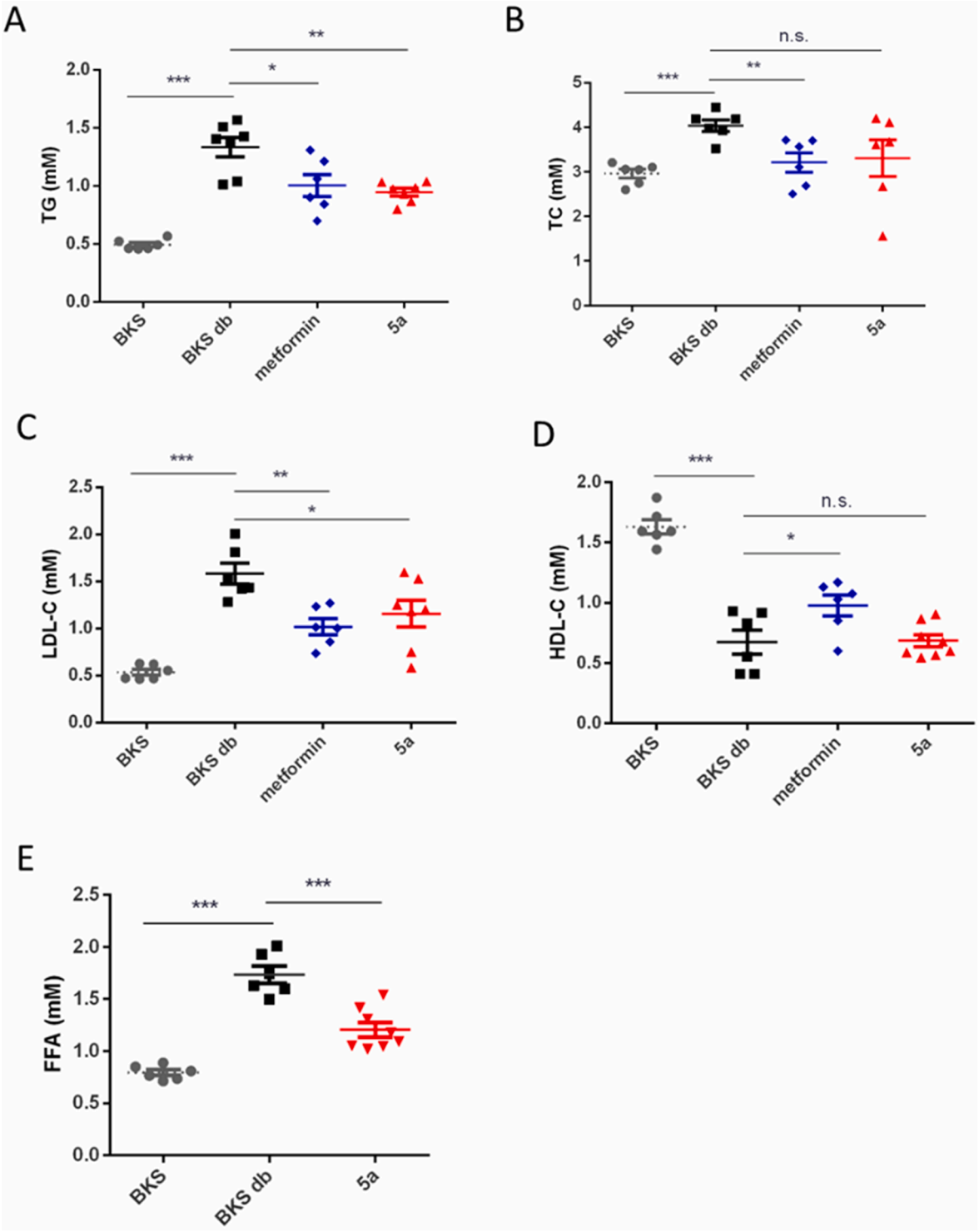

Fig. 5. Effects of compound **5a** on dyslipidemia in diabetic mice. Serum TG (A), TC (B), LDL-C (C), HDL-C (D), and circulating FFA (E) levels in normal BKS mice treated with vehicle, and in diabetic mice treated with vehicle, compound **5a**, and metformin. Data were shown as means ± SEM (n = 6–8). *$p < 0.05$, **$p < 0.01$, and ***$p < 0.001$ as indicated. n.s., not significant.

*5.1.3.2. (Z)-5-(2-bromo-3,4-dimethoxybenzylidene)imidazolidine-2,4-dione (**2b**).* Yellow solid, Yield 68%, mp: 288–290 °C, ^{1}H NMR (500 MHz, DMSO-d_6) δ: 3.74 (s, 3H), 3.88 (s, 3H), 6.52 (s, 1H), 7.11 (d, J = 8.5 Hz, 1H), 7.45 (d, J = 8.5 Hz, 1H), 10.55 (br s, 1H), 11.27 (br s, 1H)^{13}C NMR (125 MHz, DMSO-d_6) δ: 56.81, 60.48, 106.78, 112.65, 120.34, 125.99, 126.22, 129.26, 146.65, 153.83, 156.17, 165.86; HRESIMS: calc for C12H10BrN2O4 $[M-H]^-$ 324.9830, found 324.9829.

*5.1.3.3. (Z)-5-(4-hydroxy-3-methoxybenzylidene)imidazolidine-2,4-dione (**2c**).* Yellow solid, Yield 85%, mp: 216–218 °C, ^{1}H NMR (500 MHz, DMSO-d_6) δ: 3.83 (s, 3H), 6.36 (s, 1H), 6.79 (d, J = 7 Hz, 1H), 7.07 (d, J = 7 Hz, 1H), 7.11 (s, 1H), 9.46 (br s, 1H), 10.42 (br s, 1H), 11.14 (br s, 1H); ^{13}C NMR (125 MHz, DMSO-d_6) δ: 56.36, 110.34, 113.73, 116.28, 124.04, 124.87, 125.98, 148.14, 148.30, 156.29, 166.23; HRESIMS: calc for C11H9N2O4 $[M-H]^-$ 233.0633, found 233.0723.

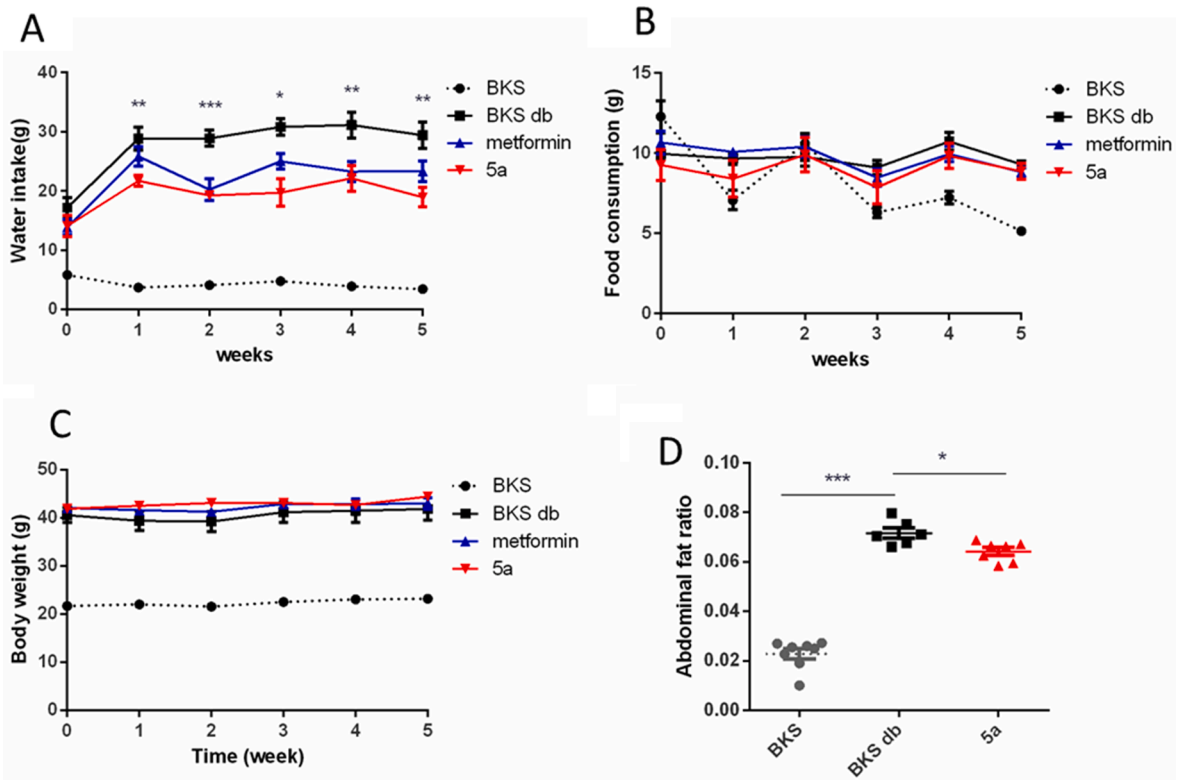

Fig. 6. Effects of compound **5a** on water intake, food intake and body weight in diabetic mice. Water intake (A), food intake (B), and body weight (C) of BKS db mice fed a normal chow diet and treated with/without compound **5a**. (D) Abdominal fat ratio of mice treated with compound **5a**. Data were shown as means ± SEM (n = 6–8). $^{*}p < 0.05$, $^{**}p < 0.01$, and $^{***}p < 0.001$, compound **5a**-treatment group *versus* vehicle-treated diabetic mice, or as indicated.

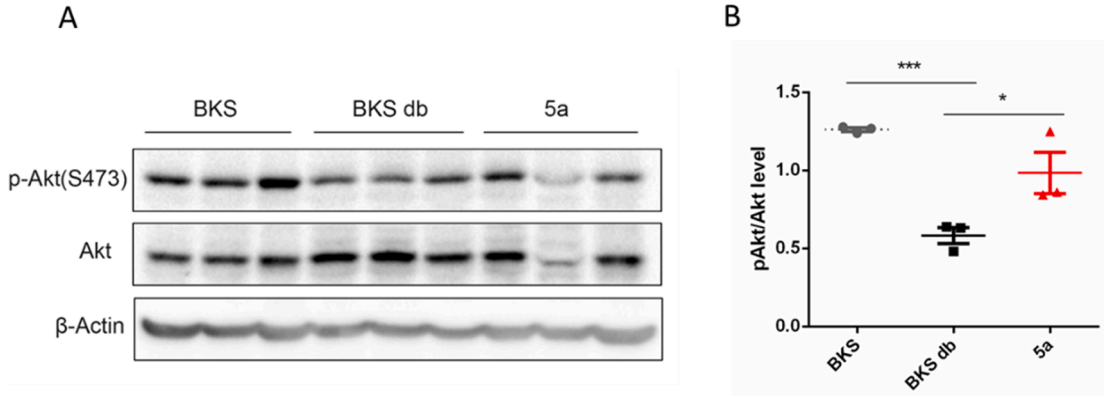

Fig. 7. Effect of compound **5a** on Akt phosphorylation in skeletal muscle tissues of diabetic mice. (A) Immunoblotting analysis of Akt phosphorylation. Skeletal muscle tissues were isolated from BKS mice treated with vehicle, and BKS db mice treated with vehicle or compound **5a**. Western blotting was used to detect Akt phosphorylation. (B) Ratio of Akt phosphorylation to total Akt. Data are expressed as means ± SEM (n = 3). $^{*}p < 0.05$ and $^{***}p < 0.001$ as indicated.

*5.1.3.4. (Z)-5-(3-bromo-4-hydroxy-5-methoxybenzylidene)imidazolidine-2,4-dione (**2d**).* Yellow solid, Yield 68%, mp: 220–222 °C, ^{1}H NMR (500 MHz, DMSO-d_6) δ: 3.87 (s, 3H), 6.32 (s, 1H), 7.10 (s, 1H), 7.39 (s, 1H); ^{13}C NMR (125 MHz, DMSO-d_6) δ: 56.90, 109.01, 110.64, 112.60, 126.47, 126.62, 146.31, 149.17, 156.26, 166.13; HRESIMS: calc for C11H8BrN2O4 $[M-H]^-$ 310.9673, found 310.9763.

*5.1.3.5. (Z)-5-(2,3-dibromo-4-hydroxy-5-methoxybenzylidene)imidazolidine-2,4-dione (**2e**).* Yellow solid, Yield 72%, mp: >300 °C, ^{1}H NMR (500 MHz, DMSO-d_6) δ: 3.93 (s, 3H), 6.48 (s, 1H), 7.09 (s, 1H), 10.64 (s, 1H), 11.31 (s, 1H); ^{13}C NMR (125 MHz, DMSO-d_6) δ: 56.81, 108.45, 112.29, 113.89, 118.34, 125.39, 129.66, 146.25, 147.69, 156.21, 165.75; HRESIMS: calc for C11H7Br2N2O4 $[M-H]^-$ 388.8778, found 388.8786.

*5.1.4. Procedure for the synthesis of TZD derivatives **5a-b***

To the solution of benzyl alcohol 9 (2.0 g, 3.6 mmol) in dry CH_2Cl_2 (20 mL) was added PCC (1.6 g, 0.73 mmol). The mixture was stirred at room temperature for 2 h. The suspension was filtered, and the filtrate was washed with H_2O (2x). The organic layer was dried over anhydrous Na_2SO_4 and concentrated in vacuo. The residue was purified by silica gel column chromatography using petroleum ether/ethyl acetate (5:1, v/v) to afford the aryl aldehyde 4 as a white solid with a yield of 78.9%.

The TZD derivative **5a** was prepared as described in 5.1.2.

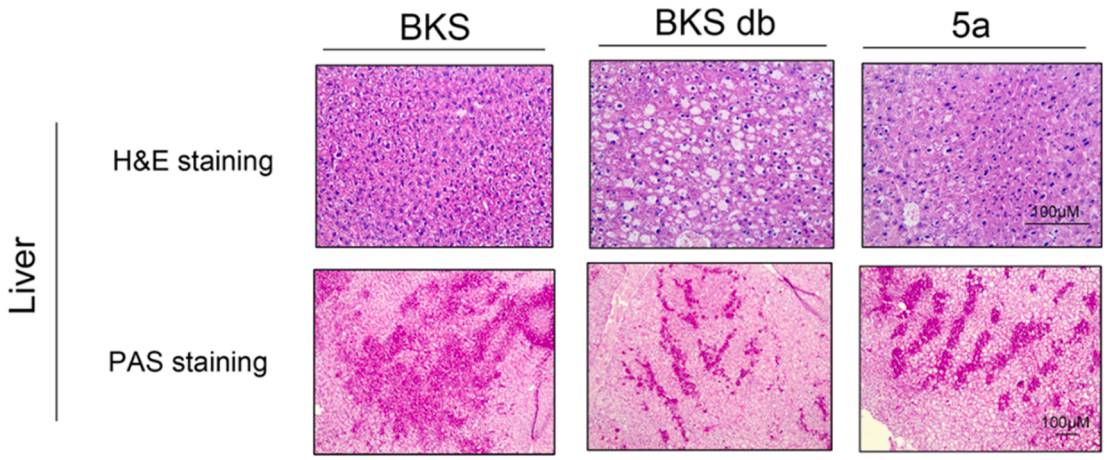

Fig. 8. Effect of compound **5a** on liver glycogen storage in diabetic mice. H&E staining and PAS staining of liver sections in normal BKS mice treated with vehicle, and diabetic BKS db mice treated with vehicle or compound **5a** (*scale bar*, 100 μm).

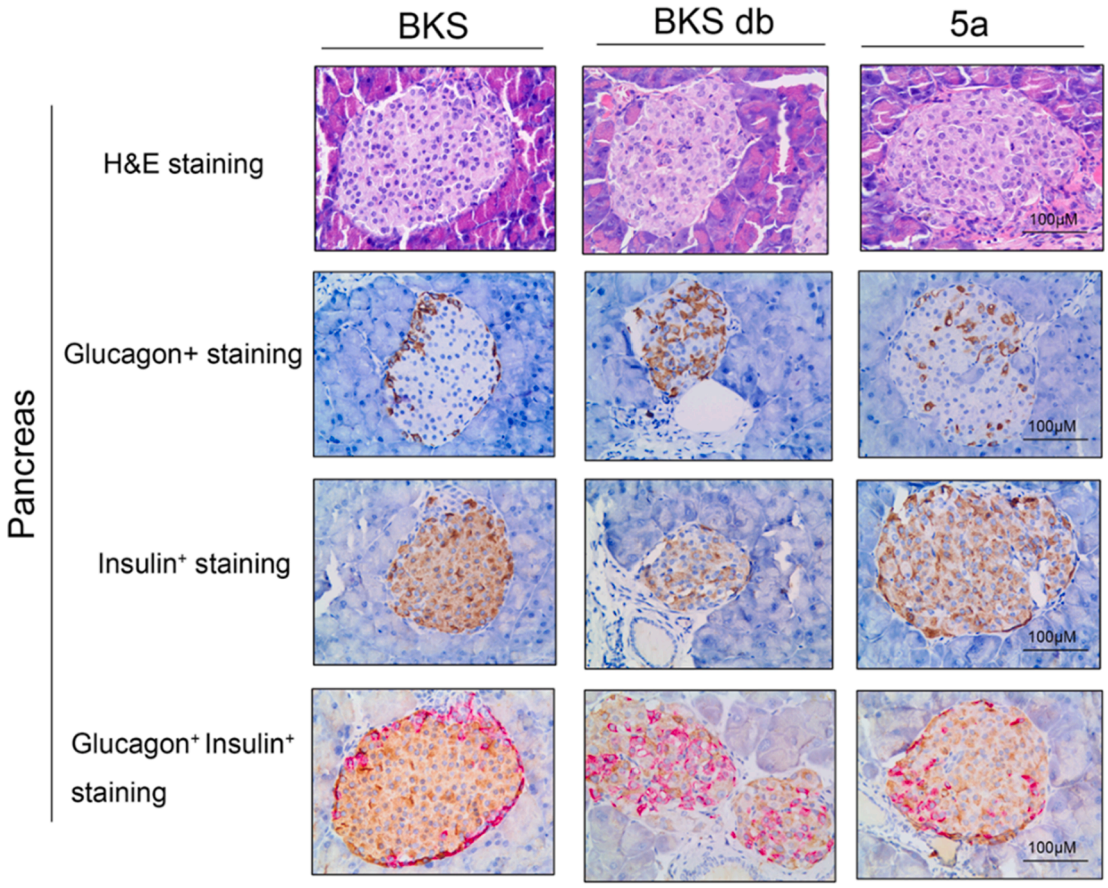

Fig. 9. Effect of compound **5a** on pancreas. H&E staining, insulin immunostaining, glucagon immunostaining, and insulin and glucagon double-immunostaining of pancreas from BKS mice treated with vehicle, and diabetic BKS db mice treated with vehicle or compound **5a** (*scale bar*, 100 μm).

*5.1.4.1. (Z)-5-(3-bromo-2-(2,3-dibromo-4,5-dimethoxybenzyl)-4,5-dimethoxybenzylidene) thiazolidine-2,4-dione (**5a**).* Yellow solid, Yield 90%, mp: 194–195 °C, ^{1}H NMR (500 MHz, DMSO-d_6) δ: 3.54 (s, 3H), 3.69 (s, 3H), 3.80 (s, 3H), 3.89 (s, 3H), 4.26 (s, 2H), 6.19 (s, 1H), 7.14 (s, 1H), 7.63 (s, 1H), 12.58 (br s, 1H); ^{13}C NMR (125 MHz, DMSO-d_6) δ: 31.25, 56.45, 56.81, 60.55, 60.82, 110.04, 111.86, 112.74, 116.95, 121.78, 122.87, 130.60, 131.28, 131.34, 136.21, 146.09, 147.64,152.64, 152.69, 168.45; HRESIMS: calc for C21H17Br3NO6S $[M-H]^-$ 647.8332, found 647.8328.

A solution of **5a** (1.3 g, 2.0 mmol) and Pd/C (50 mg, 10% palladium on carbon) was suspended in dry methanol (20 mL) and stirred at 50 °C under a 1.5 MPa hydrogen atmosphere for 5 h. After completion, the Pd/C was removed via filtration through a Celite pad. The filtrate was evaporated to dryness under reduced pressure. The resulting oil residue was chromatographed on silica gel in 20% ethyl acetate in hexane with 0.1% glacial acid to give **5b**.

*5.1.4.2. 5-(3-bromo-2-(2,3-dibromo-4,5-dimethoxybenzyl)-4,5-dimethoxybenzyl)thiazolidine-2,4-dione (**5b**).* Yellow solid, Yield 86%, mp: 92–93 °C, ^{1}H NMR (500 MHz, DMSO-d_6) δ: 2.97–3.21 (m, 2H), 3.49 (s, 3H), 3.69 (s, 3H), 3.71 (s, 3H), 3.84 (s, 3H), 4.23 (s, 2H), 4.81–4.84 (m, 1H), 6.04 (s, 1H), 7.09 (s, 1H), 12.07 (br s, 1H); ^{13}C NMR (125 MHz, DMSO-d_6) δ: 31.25, 36.04, 52.63, 56.40, 56.66, 60.55, 60.64, 112.25, 114.32, 117.06, 121.67, 122.12, 129.35, 134.54, 136.38, 145.76, 146.02, 152.48, 152.72, 172.07, 176.17; HRESIMS: calc for C21H19Br3NO6S $[M-H]^-$ 649.8489, found 649.8495.

*5.1.5. Procedure for the synthesis of TZD derivatives **8a-b***

The suspension of benzyl bromide **6** (1.0 g, 1.6 mmol), 4-ydroxybenzaldehyde (0.4 g, 3.2 mmol) and K_2CO_3 (0.3 g, 2.4 mmol) in acetone (10 mL) was stirred at room temperature overnight. The mixture was filtered, and the filtrate was evaporated in vacuo. The residue was purified by silica gel column chromatography using petroleum ether/ethyl acetate (6:1, v/v) as the eluent to afford **7**.

The TZD derivative **8a** was prepared as described in 5.1.2.

*5.1.5.1. (Z)-5-(4-(3-bromo-2-(2,3-dibromo-4,5-dimethoxybenzyl)-4,5-dimethoxyphenoxy)benzylidene)thiazolidine-2,4-dione (**8a**).* Light yellow solid, Yield 92%, mp: 207–208 °C, ^{1}H NMR (500 MHz, DMSO-d_6) δ: 3.55 (s, 3H, OCH_3), 3.69 (s, 3H), 3.76 (s, 3H), 3.90 (s, 3H), 4.16 (s, 2H), 5.13 (s, 2H), 6.06 (s, 1H), 6.85 (d, J = 7.5 Hz, 2H), 7.43 (s, 1H), 7.45 (d, J = 7.5 Hz, 2H), 7.70 (s, 1H), 12.58 (br s, 1H); ^{13}C NMR (125 MHz, DMSO-d_6) δ: 31.25, 56.15, 56.75, 60.61, 69.22, 112.64, 115.25, 116.91, 121.07, 121.31, 122.52, 126.29, 130.31, 132.24, 132.44, 133.24, 136.66, 145.80, 146.70, 152.40, 152.44, 160.09, 168.05, 168.56; HRESIMS: calc for C28H23Br3NO7S $[M-H]^-$ 753.8751, found 753.8752.

A solution of **8a** (0.76 g, 1.0 mmol) and Pd/C (30 mg, 10% palladium on carbon) was suspended in dry dichloromethane (15 mL) and stirred at 50 °C under a 1.5 MPa hydrogen atmosphere for 5 h. After completion, the Pd/C was removed via filtration through a Celite pad. The filtrate was evaporated to dryness under reduced pressure. The resulting oil residue was subjected to chromatography on silica gel in 20% ethyl acetate in hexane with 0.1% glacial acid to give **8b**.

*5.1.5.2. 5-(4-(3-bromo-2-(2,3-dibromo-4,5-dimethoxybenzyl)-4,5-dimethoxyphenoxy)benzyl)thiazolidine-2,4-dione (**8b**).* Light yellow solid, Yield 81%, mp: 102–104 °C, ^{1}H NMR (500 MHz, DMSO-d_6) δ: 2.99–3.29 (m, 2H), 3.56 (s, 3H), 3.69 (s, 3H), 3.75 (s, 3H), 3.87 (s, 3H), 4.16 (s, 2H), 4.83 (m, 1H), 5.00 (s, 2H), 6.10 (s, 1H), 6.69 (d, J = 8.5 Hz, 2H), 7.08 (d, J = 8.5 Hz, 2H), 7.38 (s, 1H), 12.03 (br s, 1H); ^{13}C NMR (125 MHz, DMSO-d_6) δ: 31.12, 36.69, 53.43, 56.09, 56.59, 60.49, 68.71, 112.59, 114.81, 116.82, 121.12, 122.23, 129.43, 130.01, 130.64, 133.65, 136.58, 145.68, 146.41, 152.24, 152.33, 157.39, 172.15, 176.16; HRESIMS: calc for C28H25Br3NO7S $[M-H]^-$ 755.8907, found 755.8925.

5.2. Molecular docking

The molecular docking study was performed using the 1.5.6 version of AutoDock combined with PyMol software. The 3D structure of compound **5a** was constructed using ChemDraw 12.0, and then the MM2 energy was minimized. The crystal structure of PTP1B was obtained from the RCSB Protein Data Bank (PDB code: 1G1H) by removing water molecules and bound ligands and adding hydrogens and Kollman charges. The domain sphere was defined by the binding site of **5a** in the crystal pose in 1G1H. Each docking experiment was performed 300 times, resulting in 300 docking conformations. All other parameters were default values of the system. The best model was selected based on the best stable energy.

5.3. Biological assays

5.3.1. Enzymatic activity assay and kinetics study

PTP1B inhibitory activities of synthetic compounds were measured using recombinant human $PTP1B_{1\text{-}321}$ proteins. Enzymatic activity methods including selectivity against other PTPs were performed as previously described [27]. In the kinetics study, a series of concentrations of pNPP (0.5, 1.0, 2.0, 4.0 and 8.0 mM) were used as PTP1B substrate in the presence of compound **5a** (1.0, 2.0, 4.0 and 8.0 μM). Lineweaver-Burk plotting of the enzymatic reaction was used to identify the inhibition type of compound **5a**.

5.3.2. Cell treatment and western blotting

C2C12 cells (a murine myoblast cell line) were cultured in DMEM containing 10% FBS and seeded in a six-well cell plate at 4×10^5 cells/well. When the cells had reached 80–90% confluence, the medium was replaced with DMEM supplemented with 10% horse serum to induce cell differentiation for an additional 4 days. After overnight starvation, the cells were treated for 8 h with different concentrations of compound **5a** (0, 0.01, 0.1, 1 and 10 μM) following insulin (100 nM) stimulation or no stimulation for 5 min.

Whole cell lysates were extracted using ice-cold RIPA buffer, and protein concentrations were measured using a BCA Protein Assay Kit. Proteins were separated on a polyacrylamide gel and transferred to and detected on PVDF membranes with specific primary antibodies. Relative band densities were detected with Western Blotting Substrate (Thermo Scientific, Waltham, MA, USA).

5.3.3. Cell permeability assay

The permeability of compound **5a** was carried out in C2C12 myotubes. The differentiated C2C12 cells were treated with **5a** (0.1 μM) and incubated for 8 h at 37 °C. The medium was then removed and the cells were washed with PBS. Then, methanol was added to fix the cells. The mixture was treated with ultrasound and the solution was collected by centrifugation. The equal amount of the internal standard (0.1 μM) was added into the solution. The resulting solution was evaporated under reduced pressure and the residue was dissolved in methanol (1 mL) for subsequent HPLC analysis (π-Nap, mobile phase: methanol/H_2O + 0.05% TFA). The gradient elution was 80% methanol to 90% methanol in 15 min followed by 90% methanol in next 15 min and 80% methanol in the next 10 min at a flow rate of 1 mL/min.

5.3.4. Cell viability test

C2C12 cells were first seeded in a 96-well plate, and after overnight incubation cells treated with compound **5a** (0.01–100 μM) for 24 h. Then cells were incubated with 10 uL CCK8 solution each well for 1 h in the 37 °C cell incubator. Finally, the absorbance was determined using a multi-well microplate reader at the wavelength of 450 nm. Cells exposed to DMSO were used as control.

5.3.5. Animal study

Animal studies were performed according to approved regulatory standards under protocol HAIFAJIZI-2013–3 (approval date: 2013-12-09; Animal Care and Use Committee of Institute of Oceanology, Chinese Academy of Sciences). 4–6 weeks male BKS.Cg-Dock7m+/+Leprdb/J mice and wild control (BKS mice) were purchased from the Model Animal Research Centre (MARC) of Nanjing University. All mice were fed *ad libitum* a normal chow diet and water. After 1 week of acclimatization, qualified diabetic mice were randomly divided into three different treatment groups (n = 8): vehicle treatment group (BKS db, 1.5% CMC-Na), metformin treatment group (metformin, 100 mg•kg^{-1} body wt•day^{-1}), and compound **5a** treatment group (**5a**, 50 mg•kg^{-1} body wt•day^{-1}). Age-matched male BKS mice (n = 8) were treated with vehicle (1.5% CMC-Na) and used as a normal control group.

Metformin and compound **5a** (in 1.5% CMC-Na) were orally administered once/daily between 08:00 and 09:00 using a cannula.

Body weight, food intake, water intake, and fasting plasma glucose levels were measured once weekly. Concentrations of total cholesterol (TC), triglycerides (TG), high-density lipoprotein-cholesterol (HDL-C), low-density lipoprotein-cholesterol (LDL-C), and circular free fatty acid (FFA) were measured by referring to the protocols from Nanjing Jiancheng Bioengineering Institute (Nanjing, China). After 6 weeks of feeding, the mice were executed by decapitation after 15 min of the insulin injection, and the blood samples were drawn from orbits. The animal tissues were dissected and quickly frozen in liquid N_2 for subsequent experiments. The animal treatment of compound **5a** were conducted during the same period according to previous studies [37], so they shared the same control group, model group and metformin treatment group.

5.3.6. *Histological analysis*

Samples of mouse liver and pancreas were fixed in formalin and embedded in paraffin. Paraffin sections with a thickness of 5 μm were prepared for subsequent analysis. Morphological changes were observed by staining liver and pancreas sections with hematoxylin and eosin (H&E). Periodic acid-Schiff (PAS) staining was used to detect liver glycogen storage. Pancreas sections were incubated with insulin antibody and/or glucagon antibody (Abcam) overnight at 4 °C to detect islet β-cells and/or α-cells.

Declaration of Competing Interest

The authors have declared no conflict of interest.

Acknowledgements

This study was supported by grants from NSFC-Shandong Joint Fund (U1706213).

References

[1] http://www.diabetesatlas.org/.
[2] N.K. Tonks, C.D. Diltz, E.H. Fischer, Purification of the major protein-tyrosine-phosphatases of human placenta, J. Biol. Chem. 263 (1988) 6722–6730.
[3] K.A. Kenner, E. Anyanwu, J.M. Olefsky, J. Kusari, Protein-tyrosine phosphatase 1B is a negative regulator of insulin- and insulin-like growth factor-I-stimulated signaling, J. Biol. Chem. 271 (1996) 19810–19816.
[4] J.C. Byon, A.B. Kusari, J. Kusari, Protein-tyrosine phosphatase-1B acts as a negative regulator of insulin signal transduction, Mol. Cell. Biochem. 182 (1998) 101–108.
[5] M. Elchebly, P. Payette, E. Michaliszyn, W. Cromlish, S. Collins, A.L. Loy, D. Normandin, A. Cheng, J. Himms-Hagen, C.C. Chan, C. Ramachandran, M. J. Gresser, M.L. Tremblay, B.P. Kennedy, Increased insulin sensitivity and obesity resistance in mice lacking the protein tyrosine phosphatase-1B gene, Science 283 (1999) 1544–1548.
[6] S. Walchli, M.L. Curchod, R.P. Gobert, S. Arkinstall, R. Hooft van Huijsduijnen, Identification of tyrosine phosphatases that dephosphorylate the insulin receptor. A brute force approach based on “substrate-trapping” mutants, J. Biol. Chem. 275 (2000) 9792–9796.
[7] S.G. Julien, N. Dube, M. Read, J. Penney, M. Paquet, Y. Han, B.P. Kennedy, W. J. Muller, M.L. Tremblay, Protein tyrosine phosphatase 1B deficiency or inhibition delays ErbB2-induced mammary tumorigenesis and protects from lung metastasis, Nat. Genet. 39 (2007) 338–346.
[8] L.Y. Zheng, D.X. Zhou, J. Lu, W.J. Zhang, D.J. Zou, Down-regulated expression of the protein-tyrosine phosphatase 1B (PTP1B) is associated with aggressive clinicopathologic features and poor prognosis in hepatocellular carcinoma, Biochem. Biophys. Res. Commun. 420 (2012) 680–684.
[9] J.R. Beck, A. Lawrence, A.S. Tung, E.N. Harris, C.I. Stains, Interrogating endogenous protein phosphatase activity with rationally designed chemosensors, ACS Chem. Biol. 11 (2016) 284–290.
[10] V.V. Vintonyak, A.P. Antonchick, D. Rauh, H. Waldmann, The therapeutic potential of phosphatase inhibitors, Curr. Opin. Chem. Biol. 13 (2009) 272–283.
[11] K.A. Lantz, S.G. Hart, S.L. Planey, M.F. Roitman, I.A. Ruiz-White, H.R. Wolfe, M. P. McLane, Inhibition of PTP1B by trodusquemine (MSI-1436) causes fat-specific weight loss in diet-induced obese mice, Obesity (Silver Spring) 18 (2010) 1516–1523.
[12] A.P. Combs, Recent advances in the discovery of competitive protein tyrosine phosphatase 1B inhibitors for the treatment of diabetes, obesity, and cancer, J. Med. Chem. 53 (2010) 2333–2344.
[13] E. Panzhinskiy, J. Ren, S. Nair, Pharmacological inhibition of protein tyrosine phosphatase 1B: a promising strategy for the treatment of obesity and type 2 diabetes mellitus, Curr. Med. Chem. 20 (2013) 2609–2625.
[14] Y. Du, Y. Zhang, H. Ling, Q. Li, J. Shen, Discovery of novel high potent and cellular active ADC type PTP1B inhibitors with selectivity over TC-PTP via modification interacting with C site, Eur. J. Med. Chem. 144 (2018) 692–700.
[15] F. Xie, F. Yang, Y. Liang, L. Li, Y. Xia, F. Jiang, W. Liu, Y. Qi, S.R. Chowdhury, D. Xie, L. Fu, Investigation of stereoisomeric bisarylethenesulfonic acid esters for discovering potent and selective PTP1B inhibitors, Eur. J. Med. Chem. 164 (2019) 408–422.
[16] N. Maheshwari, C. Karthikeyan, S.V. Bhadada, A.K. Verma, C. Sahi, N. Moorthy, P. Trivedi, Design, synthesis and biological evaluation of some tetrazole acetamide derivatives as novel non-carboxylic PTP1B inhibitors, Bioorg. Chem. 92 (2019), 103221.
[17] J.L. Tian, X.J. Liao, Y.H. Wang, X. Si, C. Shu, E.S. Gong, X. Xie, X.L. Ran, B. Li, Identification of cyanidin-3-arabinoside extracted from blueberry as a selective protein tyrosine phosphatase 1B inhibitor, J. Agric. Food Chem. 67 (2019) 13624–13634.
[18] P.H. Nguyen, B.T. Zhao, M.Y. Ali, J.S. Choi, D.Y. Rhyu, B.S. Min, M.H. Woo, Insulin-mimetic selaginellins from Selaginella tamariscina with protein tyrosine phosphatase 1B (PTP1B) inhibitory activity, J. Nat. Prod. 78 (2015) 34–42.
[19] J. Zhou, N. Sun, H. Zhang, G. Zheng, J. Liu, G. Yao, Rhodomollacetals A-C, PTP1B Inhibitory Diterpenoids with a 2,3:5,6-Di-seco-grayanane Skeleton from the Leaves of Rhododendron molle, Org. Lett. 19 (2017) 5352–5355.
[20] T. Shi, E.M.K. Wijeratne, C. Solano, A.J. Ambrose, A.B. Ross, C. Norwood, C. K. Orido, T. Grigoryan, J. Tillotson, M. Kang, G. Luo, B.M. Keegan, W. Hu, B.S. J. Blagg, D.D. Zhang, A.A.L. Gunatilaka, E. Chapman, An isoform-selective PTP1B inhibitor derived from nitrogen-atom augmentation of radicicol, Biochemistry 58 (2019) 3225–3231.
[21] Y. Zhao, M.X. Chen, K.T. Kongstad, A.K. Jager, D. Staerk, Potential of Polygonum cuspidatum root as an antidiabetic food: dual high-resolution alpha-glucosidase and PTP1B inhibition profiling combined with HPLC-HRMS and NMR for identification of antidiabetic constituents, J. Agric. Food Chem. 65 (2017) 4421–4427.
[22] P.A. Elzahhar, R. Alaaeddine, T.M. Ibrahim, R. Nassra, A. Ismail, B.S.K. Chua, R. L. Frkic, J.B. Bruning, N. Wallner, T. Knape, A. von Knethen, H. Labib, A.F. El-Yazbi, A.S.F. Belal, Shooting three inflammatory targets with a single bullet: novel multi-targeting anti-inflammatory glitazones, Eur. J. Med. Chem. 167 (2019) 562–582.
[23] K.M. Darwish, I. Salama, S. Mostafa, M.S. Gomaa, M.A. Helal, Design, synthesis, and biological evaluation of novel thiazolidinediones as PPARgamma/FFAR1 dual agonists, Eur. J. Med. Chem. 109 (2016) 157–172.
[24] F.A.K. Khan, K.S. Jadhav, R.H. Patil, D.B. Shinde, R.B. Arote, J.N. Sangshetti, Biphenyl tetrazole-thiazolidinediones as novel bacterial peptide deformylase inhibitors: synthesis, biological evaluations and molecular docking study, Biomed. Pharmacother. 83 (2016) 1146–1153.
[25] A. Gandini, M. Bartolini, D. Tedesco, L. Martinez-Gonzalez, C. Roca, N.E. Campillo, J. Zaldivar-Diez, C. Perez, G. Zuccheri, A. Miti, A. Feoli, S. Castellano, S. Petralla, B. Monti, M. Rossi, F. Moda, G. Legname, A. Martinez, M.L. Bolognesi, Tau-centric multitarget approach for Alzheimer’s disease: development of first-in-class dual glycogen synthase kinase 3beta and tau-aggregation inhibitors, J. Med. Chem. 61 (2018) 7640–7656.
[26] E.A. Gale, Lessons from the glitazones: a story of drug development, Lancet 357 (2001) 1870–1875.
[27] X. Fan, N.J. Xu, J.G. Shi, Bromophenols from the Red Alga Rhodomela confervoides, J. Nat. Prod. 66 (2003) 455–458.
[28] B. Jiang, S. Guo, D. Shi, C. Guo, T. Wang, Discovery of novel bromophenol 3,4-dibromo-5-(2-bromo-3,4-dihydroxy-6-(isobutoxymethyl)benzyl)benzene-1,2-diol as protein tyrosine phosphatase 1B inhibitor and its anti-diabetic properties in C57BL/KsJ-db/db mice, Eur. J. Med. Chem. 64 (2013) 129–136.
[29] J. Handzlik, E. Szymanska, S. Alibert, J. Chevalier, E. Otrebska, E. Pekala, J. M. Pages, K. Kiec-Kononowicz, Search for new tools to combat Gram-negative resistant bacteria among amine derivatives of 5-arylidenehydantoin, Bioorg. Med. Chem. 21 (2013) 135–145.
[30] G. Bruno, L. Costantino, C. Curinga, R. Maccari, F. Monforte, F. Nicolo, R. Ottana, M.G. Vigorita, Synthesis and aldose reductase inhibitory activity of 5-arylidene-2,4-thiazolidinediones, Bioorg. Med. Chem. 10 (2002) 1077–1084.
[31] Z. Xia, C. Knaak, J. Ma, Z.M. Beharry, C. McInnes, W. Wang, A.S. Kraft, C.D. Smith, Synthesis and evaluation of novel inhibitors of Pim-1 and Pim-2 protein kinases, J. Med. Chem. 52 (2009) 74–86.
[32] M.V. Reddy, C. Ghadiyaram, S.K. Panigrahi, S. Hosahalli, L.N. Mangamoori, Diphenylether derivative as selective inhibitor of protein tyrosine phosphatase 1B (PTP1B) over t-cell protein tyrosine phosphatase (TCPTP) identified through virtual screening, Mini Rev. Med. Chem. 13 (2013) 1602–1606.
[33] A.R. Saltiel, C.R. Kahn, Insulin signalling and the regulation of glucose and lipid metabolism, Nature 414 (2001) 799–806.
[34] A.D. Mooradian, Dyslipidemia in type 2 diabetes mellitus, Nat. Clin. Pract. Endocrinol. Metab. 5 (2009) 150–159.
[35] J.R. Testa, P.N. Tsichlis, AKT signaling in normal and malignant cells, Oncogene 24 (2005) 7391–7393.
[36] A.K. Rines, K. Sharabi, C.D. Tavares, P. Puigserver, Targeting hepatic glucose metabolism in the treatment of type 2 diabetes, Nat. Rev. Drug Discov. 15 (2016) 786–804.
[37] C. Li, J. Luo, S.J. Guo, X.L. Jia, C.L. Guo, X.Q. Li, Q. Xu, D.Y. Shi, Highly selective protein tyrosine phosphatase inhibitor, 2,2′,3,3′-tetrabromo-4,4′,5,5′-tetrahydroxydiphenylmethane, ameliorates type 2 diabetes mellitus in BKS db mice, Mol. Pharm. 16 (2019) 1839–1850.